Journal of
Composites Science

MDPI

Article

Prediction of Failure in Ceramic Matrix Composites Using Damage-Based Failure Criterion

Neraj Jain [1,*] and Dietmar Koch [2]

[1] German Aerospace Centre, Institute of Structures and Design, 70569 Stuttgart, Germany
[2] Institute of Materials Resource Management, University of Augsburg, 86159 Augsburg, Germany; dietmar.koch@mrm.uni-augsburg.de
* Correspondence: Neraj.Jain@dlr.de

Received: 10 November 2020; Accepted: 2 December 2020; Published: 7 December 2020

Abstract: This paper presents a damage-based failure criterion and its implementation in order to predict failure in ceramic matrix composites (CMC) manufactured via filament winding. The material behavior of CMCs is anisotropic and strongly depends on the angle between fiber orientation and loading direction. The inelastic behavior of laminates with different fiber orientations under tension and shear is modeled with the help of continuum damage mechanics. The parameters required for the damage model are obtained from a standard tensile and shear test. An isotropic damage law determines the evolution of damage in thermodynamic space and considers the interaction of damage parameters in different principal material directions. A quadratic damage-based failure criterion inspired by the Tsai-Wu failure criterion is proposed. Failure stress and strain can be predicted with higher accuracy compared to the Tsai-Wu failure criterion in stress- or strain-space. The use of the proposed damage limits allows designing a CMC component based on the microstructural phenomenon of stiffness loss. With the help of results obtained from modeling and experiments, fracture mechanics during the Iosipescu-shear test of CMCs and its capability to determine the shear strength of the material is discussed.

Keywords: continuum damage mechanics; damage-based failure criterion; woven CMC

1. Introduction

Continuous fiber reinforced ceramic matrix composites (CMC) are being used in many fields, such as aeronautical, aerospace and automobile, because of their excellent thermomechanical properties at high temperatures and relatively low density when compared to their metallic counterparts [1–5]. Filament winding technology is one of the preforming methods which is employed to manufacture CMCs with rotational symmetry axis and application-tailored fiber orientation [6,7]. Two such CMCs that are manufactured at German Aerospace Centre (DLR) are C/C–SiC (Institute of Structures and Design) and WHIPOX™ (Institute of Materials Research) via filament winding.

Despite the presence of a brittle ceramic matrix in CMCs, this material class exhibits inelastic behavior because of energy dissipating mechanisms, such as matrix cracking and fiber–matrix interphase debonding [8,9]. Many damage models have been proposed in the literature to describe the inelastic behavior of CMCs. The micromechanics-based approach proposed by Lamon [10] delivers accurate results in predicting damage but requires model parameters which can only be obtained from the individual constituents of a CMC, namely fiber and matrix. However, in a complex matrix system like C–SiC, the material under consideration, it is challenging to evaluate the effective properties of a representative matrix material. Even the bulk material properties of a monolithic matrix material cannot be used because the matrix undergoes massive changes when employed for a fiber-reinforced material due, to effects such as hindered matrix shrinkage during the manufacturing process [11]. Baranger has

summarized damage models and the rupture criterion at different microscopic scales in his work where stress and strain are used as limits to design a CMC component [12]. A thermodynamical formulation of the anisotropic damage model is discussed by Wulfinghoff et al. by linking crack channels and pores with degradation in properties [13]. Models describing the damage of a homogenous CMC material at the macro-level have also been a topic of investigation for many researchers [14–18]. These models describe damage as the degradation of stiffness in principal material directions as the load increases. A model with a similar theoretical background of continuum damage mechanics is proposed by Barbero [19] and is implemented in the current work because of the lower number of tests required in parameter-identification for the model. Apart from that, testing norms for CMCs already exist for these required tests.

The above-mentioned continuum damage models successfully describe non-linearity in the material but do not explicitly predict the final failure of composite. A failure criterion is required in order to predict the failure stress or strain of a laminate. Several physics-based and empirical failure criteria for fiber-reinforced composites have been reported in the literature and are summarized in the World Wide Failure Exercise (WWFE) [20]. Failure criteria based on micromechanics are not appropriate in the case of some CMCs because of the same above-mentioned reasons as for damage models. Apart from that, phenomenological criteria such as Cuntze and Puck require material parameters based on tests conducted on unidirectional (UD) ply, which is not possible in the case of the wound materials under consideration. For these reasons, the Tsai-Wu failure criterion is found to be the most appropriate as the parameters required for its implementation can be obtained from standardized tests in case of CMCs. The availability of standardized tests for CMCs is not trivial. For example, there are no standardized combined shear–compression tests for CMCs to obtain the required friction parameter for the Cuntze criterion [21]. Based on the strength of tensile samples with different fiber orientations, failure stresses and strains for a virtual UD ply are evaluated. However, Tsai-Wu failure has its shortcomings as it is not able to differentiate between failure modes. The Tsai-Wu failure criterion is extended by Paepegem in order to determine the stress component responsible for the failure of a ply [22]. A quantitative comparison of direction-dependent failure modes is, though, not demonstrated in his work. Tushtev et al. implemented a damage model with a failure criterion based on thermodynamic forces for a 2D-woven C/C composite [23]. A similar damage-dependent quadratic failure criterion is proposed by Yang et al. as well, where strength predictions are made for a 2D-woven C/SiC material [24]. The proposed model is applicable not only on laminates with woven fiber architecture, but also on CMCs with wound fiber architecture.

In the current work, an attempt has been made to combine continuum damage mechanics with a damage-based quadratic failure criterion. Although only tensile and shear tests were considered for the materials under consideration, the proposed failure criterion allows the integration of damage under compression if the damage behavior varies under tension and compression. A damage-based criterion has the advantage over the Tsai-Wu failure criterion in stress- or strain-space that it can give an insight into the fracture mechanics of the laminate because of its direction dependency. It can be used for designing CMC structures where damage, i.e., loss of stiffness in different directions, can be considered as a design limit instead of strength or strain. In this way, an empirical damage-based failure criterion based on macro-mechanics can deliver more information about phenomenon at the micro-level through damage variables which can be correlated to properties like crack density within a material. The proposed model exhibits an advantage over other empirical failure criteria as it can determine the responsible component in the damage-space, and thus can predict the failure mode in laminates with varying fiber orientations.

2. Materials and Methods

2.1. Materials and Testing

Two CMC materials are investigated in the current work which are manufactured via filament winding at different facilities of German Aerospace Centre (DLR): C/C–SiC and WHIPOX™. C/C–SiC stands for carbon fiber-reinforced composite where the matrix is made up of carbon (C) and silicon carbide (SiC). This material has been under development at Institute of Structures and Design (Stuttgart, Germany) since the mid-1990s for high temperature applications such as thermal protection systems for re-entry vehicles and disk brakes in the automotive industry. The manufacturing process of C/C–SiC is reported in detail in past publications from the institute [25,26]. The material and the test data used in this work are taken from the work of Breede [27] where C/C–SiC was manufactured via filament winding for nozzle applications. In order to characterize the material, tensile tests and shear tests were carried out on laminates with varying fiber orientations. Woven prepregs and braided fiber architecture can also be employed in the manufacturing process based on the geometry and application of the final component. Since the nozzle geometry is axisymmetric in nature, filament winding was employed to prepare the fiber preform.

WHIPOX™ stands for 'wound highly porous oxide material' and is manufactured at the Institute of Materials Research at DLR in Cologne, Germany. It is an Al_2O_3 fiber-reinforced Al_2O_3 matrix composite and also includes a filament winding step in its manufacturing process. The detailed manufacturing process of WHIPOX™ can be found elsewhere [6,28,29]. The experimental results used in this paper are taken from the work of Shi [30] where he performed a thorough characterization of WHIPOX™ in order to evaluate the mechanical properties of laminates with different fiber orientations. The tensile and shear tests for both the materials were conducted at the Institute of Structures and Design, DLR, Stuttgart.

2.2. Modeling Approach

2.2.1. Continuum Damage Model

A progressive damage model based on the approach proposed by Barbero [31] is implemented for a 2D plane-stress case. The model incorporates a reduction of stiffness in an anisotropic material with increasing load to represent the loss of stiffness in a material due to the presence of cracks. In the current work, three independent scalar damage variables (d_1, d_2 and d_{12}) are used which are associated with the Young's (E_1 and E_2) and shear moduli (G_{12}) of the material, respectively. The compliance tensor can be evaluated from a free energy density function, which is given by:

$$\chi = \frac{\sigma_1^2}{2(1-d_1)E_1} + \frac{\sigma_2^2}{2(1-d_2)E_2} + \frac{\sigma_{12}^2}{2(1-d_{12})G_{12}} + \frac{\nu_{12}\sigma_1\sigma_2}{E_1} \tag{1}$$

The partial derivative gives the compliance tensor S of the damaged material in Voigt notation:

$$S = \frac{\partial \chi}{\partial \sigma} = \begin{bmatrix} \frac{1}{(1-d_1)E_1} & \frac{\nu_{21}}{E_2} & 0 \\ \frac{\nu_{12}}{E_1} & \frac{1}{(1-d_2)E_2} & 0 \\ 0 & 0 & \frac{1}{(1-d_{12})G_{12}} \end{bmatrix} \tag{2}$$

A damage surface (g^d) in the thermodynamic force space is proposed by Barbero, where thermodynamic forces (Y) are given by:

$$Y = \frac{\partial \chi}{\partial d} \tag{3}$$

The damage surface (g^d) can be considered as analogous to the yield surface in the plasticity theory and is given by:

$$g^d = \sqrt{J_1 Y_1^2 + J_2 Y_2^2 + J_{12} Y_{12}^2} - (\gamma + \gamma_0) \tag{4}$$

where

J_i = internal material constants
Y_i = thermodynamic forces
γ = damage evolution variable
γ_0 = damage threshold

It has to be mentioned at this point that the H terms (internal material constants) proposed by Barbero [19] are not included in this work. H terms allow differentiation between the material behaviors under tension and compression, but this term is neglected in the current work. It is known to the authors that CMCs generally behave differently under tension and compression, but due to a lack of the test data (stress–strain curve from a pure compression test) required for determination of the damage parameter, the behavior is considered to be linear elastic under compression. It was observed during the compression tests performed on WHIPOX™ [30] and C/C [32] that the samples either fail due to buckling or delamination in the sample. Due to the presence of buckling during the compression test, it is difficult to separate material non-linearity from geometrical non-linearity in the compression test.

The evolution of the damage surface (g^d) can be explained with the help of Figure 1. There is no damage until the thermodynamic forces remain in the elastic domain till γ is less than the threshold values of γ_0. As the load on the material increases, the thermodynamic forces increase and leave the elastic domain of the material. Based on the damage evolution law, accumulated damage is evaluated in a particular stress state. In the current work, an exponential law is used to determine the evolution of damage with increasing load, and is given by the following equation:

$$\gamma = c_1\left(1 + \exp\left(\frac{\delta}{c_2}\right)\right) \tag{5}$$

where

δ is the kinematic variable and is always greater than zero to ensure the positive value of damage.
c_1 and c_2 are hardening parameters obtained after curve fitting from experimental data.

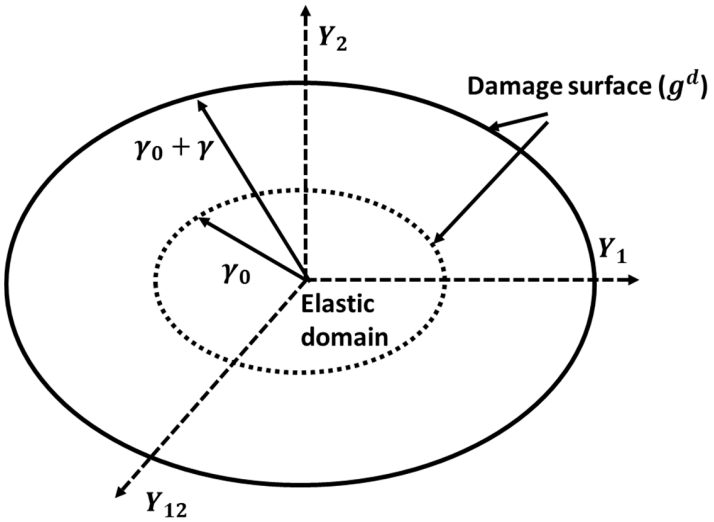

Figure 1. 2D representation of thermodynamic force space where no damage occurs in the elastic domain and the damage surface evolves based on the damage evolution law.

The damage hardening law used in the work is isotropic in nature, i.e., there is uniform expansion of the damage surface because there are insufficient test data to determine parameters for an anisotropic hardening law. It is also important to mention that the damage surface reduces to a Tsai-Wu surface in the stress-space. Analogous to the interaction of stress components in the Tsai-Wu failure criterion, the damage surface considers the interaction of damage components in the thermodynamic force space. The material parameters J_1, J_2, J_{12}, γ_0, c_1 and c_2 are obtained after performing curve fitting on experimental data, as discussed in detail in [19,33]. Other constitutive equations required for the evaluation of the elastic tangent stiffness matrix and the return mapping algorithm employed for its implementation in the commercial finite element software, ANSYS Workbench 2020R1, are based on the approach proposed by Barbero [31]. Two-dimensional 4-noded shell elements are used to perform finite element analysis and demonstrate the damage model in ANSYS. Boundary conditions are given in such a way that the sample represents pure tension and pure shear case in order to compare the results directly with the experimental results.

2.2.2. Tsai-Wu Failure Criterion

The continuum damage model discussed in the previous section determines the loss of stiffness in laminates but does not predict failure of the material. A failure criterion needs to be defined in order to predict the stress or strain at failure for a laminate. The Tsai-Wu failure equation is an empirical equation which can be used to predict stress or strain based on its implementation in stress- or strain-space, respectively. In this section, both these spaces with the extension of the Tsai-Wu criterion in the damage-space are discussed.

Stress- and Strain-Space

The Tsai-Wu failure surface in the stress-space is given by [34]:

$$F_i\sigma_i + F_{ij}\sigma_i\sigma_j = 1 \tag{6}$$

where $i, j = 1, 2, \ldots, 6$, and F_i and F_{ij} are strength tensors of the second and fourth rank, respectively. Their values are obtained from the strength of a UD ply in different loading directions and $\sigma_{i,j}$ are corresponding stress components. A safety ratio (R) is integrated in Equation (6) and the equation can be reformulated as [35]:

$$\left(F_{ij}\sigma_i\sigma_j\right)R^2 + (F_i\sigma_i)R - 1 = 0 \tag{7}$$

The positive root of the quadratic equation gives a strength ratio which can be used as a linear scaling factor in order to design a certain component based on the Tsai-Wu failure criterion. In the current work, a plane stress case is considered, where Equation (6) reduces to:

$$F_1\sigma_1 + F_2\sigma_2 + F_{11}\sigma_1^2 + F_{22}\sigma_2^2 + F_{66}\sigma_{12}^2 + 2F_{12}\sigma_1\sigma_2 = 1 \tag{8}$$

Apart from F_{12}, all other parameters can be evaluated directly from the tensile, compressive and shear strengths of a unidirectional (UD) ply. The value of F_{12} has to be determined from a bi-axial tensile test, where equal tensile loads are applied on two principal material axes of a UD layer, avoiding any shear load on the lamina. However, due to difficulty in performing such a test, certain empirical equations are proposed for the evaluation of F_{12} in Ref. [36]. In the work of Narayanswami et al. [37], the results show that the value of interaction parameter F_{12} can often be taken as zero for composite materials with low percentages of error when compared to experimentally determined F_{12}. Due to the lack of such bi-axial tests for both the materials under consideration, F_{12} was taken as zero for both the materials. Equation (8) then reduces to:

$$F_1\sigma_1 + F_2\sigma_2 + F_{11}\sigma_1^2 + F_{22}\sigma_2^2 + F_{66}\sigma_{12}^2 = 1 \tag{9}$$

The strength ratio can then be evaluated by solving the following quadratic equation for R:

$$(F_1\sigma_1 + F_2\sigma_2)R + \left(F_{11}\sigma_1^2 + F_{22}\sigma_2^2 + F_{66}\sigma_{12}^2\right)R^2 - 1 = 0 \tag{10}$$

The Tsai-Wu failure criterion can be implemented in strain-space with the help of the strain limit values of a UD ply. The quadratic failure equation, then, is given by [35]:

$$(G_1\varepsilon_1 + G_2\varepsilon_2)R + \left(G_{11}\varepsilon_1^2 + G_{22}\varepsilon_2^2 + G_{66}\varepsilon_{12}^2\right)R^2 - 1 = 0 \tag{11}$$

where G_i and G_{ij} are calculated in the exact same way as in the stress-space. The strain limit values from tests performed in different loading directions are used to determine these parameters. The criterion in the strain-space might be preferred in a laminate because global strains are uniform in all the plies, or vary linearly over the thickness of a laminate.

Damage-Space

The empirical nature of the quadratic equation proposed by Tsai-Wu has the advantage that it can be used in different spaces. As discussed in the previous section, the damage evolution is determined in the thermodynamic force space. This suggests that this quadratic equation can be used in the damage-space as well in order to define failure based on damage or loss of stiffness in different principal material directions in a particular ply. In a damage-based failure criterion, critical damage values in each direction are used to evaluate the parameters for the quadratic equation. Critical damage (d_{max}) in a ply is given by:

$$d_{max} = 1 - \frac{E_{failure}}{E} \tag{12}$$

where $E_{failure}$ is the secant modulus at failure or the ratio of failure stress to failure strain, and E is the Young's modulus or shear modulus, depending on the test. Analogous to strength parameters in the stress-space, parameters in the damage-space are evaluated as shown below:

$$H_1 = \frac{1}{d_{1max}^T} - \frac{1}{d_{1max}^C} \tag{13}$$

$$H_{11} = \frac{1}{d_{1max}^T\, d_{1max}^C} \tag{14}$$

$$H_2 = \frac{1}{d_{2max}^T} - \frac{1}{d_{2max}^C} \tag{15}$$

$$H_{22} = \frac{1}{d_{2max}^T\, d_{2max}^C} \tag{16}$$

$$H_{66} = \frac{1}{(d_{12max})^2} \tag{17}$$

where superscripts 'T' and 'C' represent tension and compression, respectively. The quadratic failure criterion in the damage-space for a plane stress case is given as:

$$H_1 d_1 + H_2 d_2 + H_{11} d_1^2 + H_{22} d_2^2 + F_{66} d_{12}^2 = 1 \tag{18}$$

where d_1, d_2 and d_{12} are obtained from the damage model for any given load. It is important to mention that damage cannot take any negative values like in stress- or strain-space. However, the inelastic behavior of material is known to be different under tension and compression [30]. For this particular reason, damage values under compression are taken as negative for the sake of the convexity of the quadratic equation, but physically, damage can only be positive according to the second law of

thermodynamics. Since there were no data available under compression, the critical damage values under compression were assumed to be same as under tension. A strength ratio can be calculated in the damage-space as well:

$$(H_1 d_1 + H_2 d_2)R + \left(H_{11} d_1^2 + H_{22} d_2^2 + F_{66} d_{12}^2\right)R^2 - 1 = 0 \tag{19}$$

The R value obtained from the above equation is then directly multiplied with load to determine the failure stress and strain of the ply:

$$\sigma_{failure} = \sigma_{load} \cdot R \tag{20}$$

where σ_{load} is applied stress on the material and $\sigma_{failure}$ is the failure stress of the material. Similarly, failure strain $\varepsilon_{failure}$ is evaluated as:

$$\varepsilon_{failure} = \varepsilon_{load} \cdot R \tag{21}$$

where ε_{load} is the strain applied on the material. Failure stresses and strains obtained from the Tsai-Wu criterion in the stress-, strain- and damage-spaces are discussed in the next section.

3. Results and Discussion

3.1. Experimental Results

The behavior of two different materials, namely C/C–SiC and WHIPOX™, is summarized in this section. Manufacturing and testing for both the materials was performed in the framework of two dissertations at DLR. Tensile and Iosipescu shear tests were carried out for different fiber orientations in order to characterize the material. All the tests were performed at room temperature. Detailed information about the manufacturing process and testing methods for C/C–SiC and WHIPOX™ can be found in the work of Breede [27] and Shi [30], respectively. It is evident from the stress–strain curves that the material starts behaving non-linearly when the fiber orientation increases from the fiber-dominated orientation of ±15° to the matrix-dominated orientation of ±75°. Although both the materials were manufactured via filament winding, the mechanisms resulting in non-linearity in the materials are different due to their particular microstructures. C/C–SiC is a material which falls between the categories of 'weak-interphase' and 'weak-matrix' CMCs. The quasi-brittle behavior of C/C–SiC can be attributed to the pull-out of C/C blocks embedded in the SiC matrix. On the other hand, WHIPOX™ belongs to the 'weak-matrix' category where the energy is dissipated by matrix cracks present in the relatively porous material (open porosity up to 35%) [11]. The stress–strain curves under tensile and shear loadings are discussed in detail in Section 3.3.

The mechanical properties of both the materials for different fiber orientations are summarized in Tables 1 and 2. Three to five samples were tested for each fiber orientation. It is evident from both tables that the strength of the material decreases when moving from fiber-dominated fiber orientation, e.g., ±15°, to the matrix-dominated fiber orientation, e.g., ±75°. The weak matrix in both the materials is the reason behind the low strength in the matrix-dominated fiber orientations. Young's modulus, on the other hand, first decreases till ±45°, and then increases again. This effect can be attributed to the lower intralaminar shear stiffness of the material, which is discussed in detail in the next section. In the case of WHIPOX™, the effect is more prominent because of the presence of manufacturing defects in the fiber orientations of ±30°, ±45° and ±60°. During the sintering process of the material, the shrinkage of the matrix is hindered by the stiff aluminium oxide fibers, which results in pre-existing cracks within the matrix before it is tested. This effect is dominant in the above-mentioned fiber orientations and results in a relatively weaker matrix with lower stiffness when compared with other fiber orientations. This phenomenon is discussed in detail in previous work [38].

Table 1. Mechanical properties of C/C–SiC obtained from tensile and shear tests for different fiber orientations.

Property	Unit	±15°	±30°	±45°	±60°	±75°
E_x	GPa	117 ± 20	77 ± 2	32 ± 3	34 ± 3	57 ± 4
G_{xy}	GPa	27 ± 2	-	41 ± 6	-	27 ± 1
σ_x	MPa	149 ± 13	151 ± 26	95 ± 8	39 ± 5	35 ± 4
ε_x	%	0.20 ± 0.02	0.34 ± 0.06	0.70 ± 0.25	0.42 ± 0.05	0.06 ± 0.01

Table 2. Mechanical properties of WHIPOX™ obtained from tensile and shear tests for different fiber orientations.

Property	Unit	±15°	±22.5°	±30°	±45°	±60°	±67.5°	±75°
E_x	GPa	202 ± 7	198 ± 15	131 ± 9	99 ± 2	68 ± 8	141 ± 14	114 ± 14
G_{xy}	GPa	51 ± 1	55 ± 12	50 ± 11	59 ± 2	50 ± 11	55 ± 12	51 ± 01
σ_x	MPa	276 ± 5	233 ± 38	133 ± 19	96 ± 9	27 ± 3	37 ± 4	22 ± 4
ε_x	%	0.14 ± 0.01	0.12 ± 0.01	0.12 ± 0.03	0.13 ± 0.02	0.07 ± 0.01	0.03 ± 0.01	0.02 ± 0.01

The shear modulus of the fiber orientations ±15° and ±75°, in the case of C/C–SiC, is almost the same as is expected from the classic laminate theory. The same conclusion can be drawn for the fiber orientations ±15° and ±75°, ±22.5° and ±67.5°, and ±30° and 60° in the case of WHIPOX™ [30].

3.2. Elastic Behavior

In order to predict the elastic behavior of composites, homogenization methods such as rule of mixtures are usually employed. Based on the elastic properties of the individual constituents, namely fiber and matrix, the elastic properties of a composite with a definite fiber volume content can be determined. However, in the case of CMCs, the matrix properties as a constituent in the CMCs are different from the matrix as bulk material. For example, the properties of Al_2O_3 as bulk material cannot be used as representative of the matrix material in WHIPOX™ because the microstructure of Al_2O_3 in WHIPOX™ is completely different from the bulk material due to the presence of shrinkage cracks. Similarly, C/C–SiC exhibits a complex matrix system with carbon matrix embedded in the SiC regions, which makes it difficult to evaluate the properties of the representative matrix with the required accuracy. In the previous work of the authors, inverse laminate theory is successfully employed in order to evaluate the elastic properties of a virtual unidirectional (UD) layer. With the help of the elastic properties of these UD layers, the properties of laminates with different fiber orientations can be predicted with the help of classical laminate theory. The in-plane elastic properties of the virtual UD layers for both the materials are listed in Table 3.

Table 3. Elastic properties of the virtual unidirectional layer used for the evaluation of the elastic properties of laminates with varying fiber orientations.

Property	Unit	C/C–SiC	WHIPOX™ [38]
E_1	GPa	145.0	211.2
E_2	GPa	60.0	56.2
ν_{12}	-	0.2	0.2
G_{12}	GPa	9.0	40.0

The values of WHIPOX™ are taken from a previous publication [38]. In the case of C/C–SiC, the values of the UD values were evaluated from data fitting for other fiber orientations. A comparison between the values from classical laminate theory and the experimentally evaluated elastic properties is shown in Figure 2. A good agreement was found in the case of C/C–SiC. However, in the case of WHIPOX™, the Young's modulus of the sample with a ±75° winding angle is underestimated by the classical laminate theory. This discrepancy can be attributed to the elastic properties of the virtual UD

layer. As discussed in the previous section, the material exhibits shrinkage in the case of winding angles ±30°, ±45° and ±60°. However, in the case of ±75°, there are no such shrinkage cracks, and the matrix is stiffer than the matrix for other winding angles (±30°, ±45° and ±60°). This effect is discussed in detail in [38], where two different sets of elastic properties are used for the determination of the elastic properties of the laminates based on the presence of shrinkage cracks. Since the focus of the paper is on the inelastic behavior of the material, which is dominant in winding angles from ±30°to ±60°, the properties of virtual UD layers with shrinkage cracks were taken for all fiber orientations.

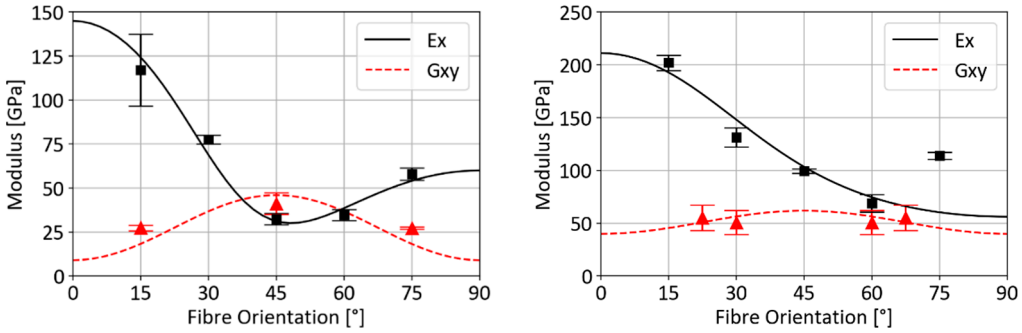

Figure 2. Comparison between the values of E_x (black squares) and G_{xy} (red triangles) with standard deviation obtained from tensile and shear tests and values evaluated from implementation of classical laminate theory on virtual UD plies for different fiber orientations for (**a**) C/C–SiC and (**b**) WHIPOX™.

3.3. Inelastic Behavior

The inelastic behavior of the materials is modeled with the help of the continuum damage model discussed in Section 2.2.1. Parameter fitting is performed for both the materials and they are listed in Table 4. The parameters J_{11}, J_{22} and J_{12} were fitted to the stress–strain curves of fiber orientations ±15°, ±75° and ±45°, respectively. The reason behind this is the dominant local stress component (σ_1, σ_2 and σ_{12}) in a particular fiber orientation, as shown in Figure 3. For example, if a global tensile load is applied on a sample with a ±15° fiber orientation, the stress gets resolved into a higher value of σ_1 and lower values of σ_2 and σ_{12}. On the other hand, in a sample with ±75°, the stress gets resolved into higher values of σ_2 and lower values of σ_1 and σ_{12}. The sample with a ±45° fiber orientation exhibits equal values of σ_1, σ_2 and σ_{12}, and therefore, is the highest contribution of σ_{12} among all the other fiber orientations. Based on this local stress contribution of stresses, the limits in thermodynamic space, J_{11}, J_{22} and J_{12}, were obtained from stress–strain curves of different fiber orientations. The shape parameters (c_1 and c_2) of the curve were fitted with the help of a ±45° tensile sample, or in other words, the material behavior under shear loading, where the material shows the maximum non-linearity.

Table 4. Damage parameters.

Property	C/C–SiC	WHIPOX™
J_{11}	15	0.1
J_{22}	45	50
J_{22}	28	10
γ_0	0.014	0.004
c_1	0.03	0.015
c_2	−0.025	−0.055

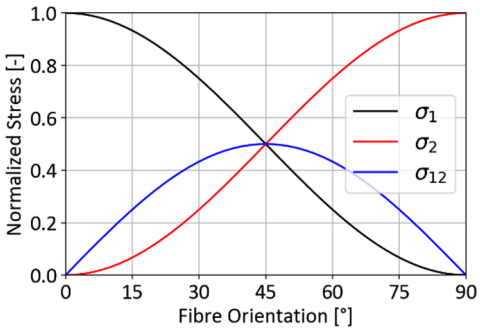

Figure 3. Normalized variation of local stress components after application of pure tensile load on a laminate with given fiber orientation.

3.3.1. Tensile Test

Figure 4 shows the comparison between experimental results and simulation results for tensile and shear tests. Three to five samples were tested for each fiber orientation but only one curve is shown for better visualization. The investigated continuum damage model is able to capture the inelastic behavior of the material for different fiber orientations. It has to be kept in mind that the continuum damage model describes the non-linearity or damage in the material, but requires a failure criterion to predict the failure stress or strain of a particular laminate. In this section, only the inelastic deformation of the material is discussed, and the failure criterion is discussed in the next section. The failure strain from the experiments was defined as load in the finite element simulation. Due to this reason, the damage model curves in Figure 4 end exactly where the experimental curves end.

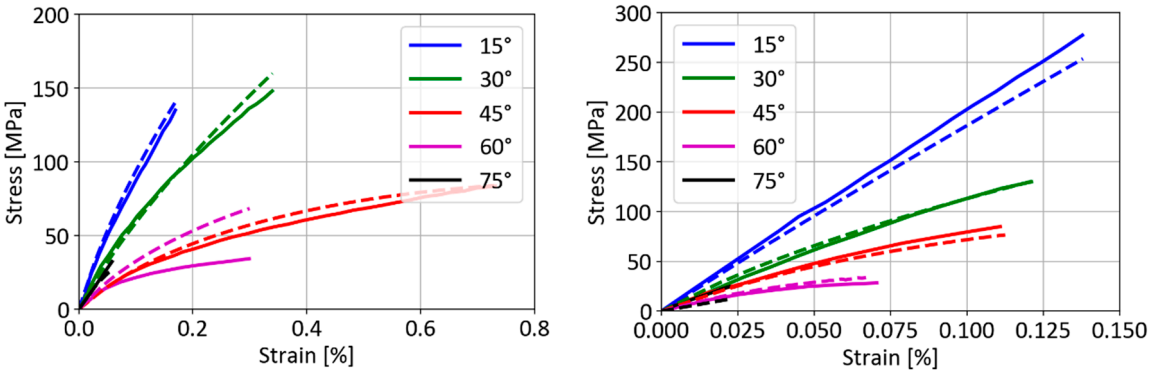

Figure 4. Comparison between stress–strain curves obtained from simulation (broken line) and tensile tests (solid line) with different fiber orientations: (**a**) C/C–SiC; (**b**) WHIPOX™.

In the case of C/C–SiC, the simulation results are in good agreement with the experimental results apart from the winding angle of ±60°. If the global load on a sample with a ±60° fiber orientation is resolved into local stress components, σ_2 and σ_{12} are present in the material with a small contribution of σ_1. This phenomenon can be explained with the help of Figures 5 and 6. In Figure 5, the development of damage components (d_1, d_2 and d_{12}) with respect to the global loading strain is plotted. In the case of ±15°, the load is mostly carried by fibers and damage is noticed only in 1-direction (d_1). d_2 is zero and there is a small amount of d_{12} present in the sample. On the other hand, in the case of ±75°, the damage is only in the matrix-dominant 2-direction where only d_2 plays a role in the failure of the sample. For the sample with a ±45° fiber orientation, the major load is carried by the shear stiffness of the material, and there is a significant amount of d_{12} in the laminate. However, in the case of ±30°, there is the presence of d_1 and d_{12}, suggesting that there is damage in both the 1-direction and 12-direction. Similarly, for ±60°, the presence of d_2 and d_{12} suggests that there is damage in the 2-direction and the

12-direction. In other words, the combined effect of the damage indices is responsible for the failure in these laminates.

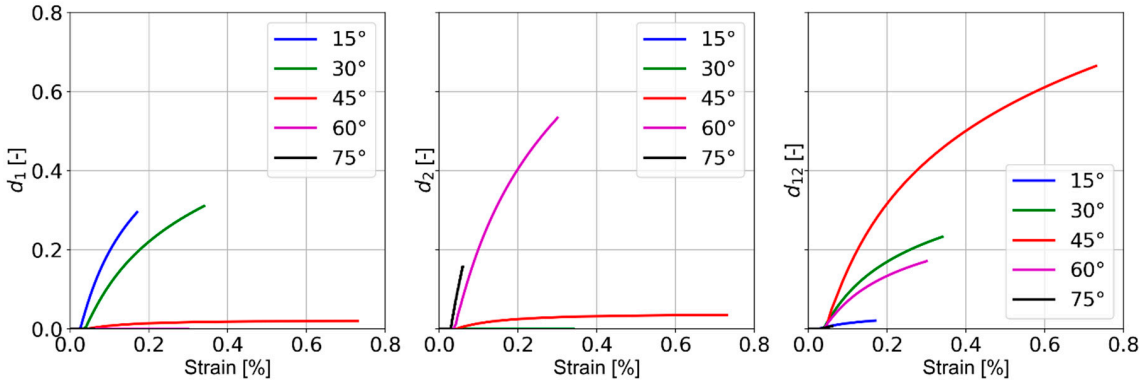

Figure 5. Comparison between damage values from the model with global strain values obtained from tensile tests for C/C–SiC with (**a**) d_1, (**b**) d_2 and (**c**) d_{12}.

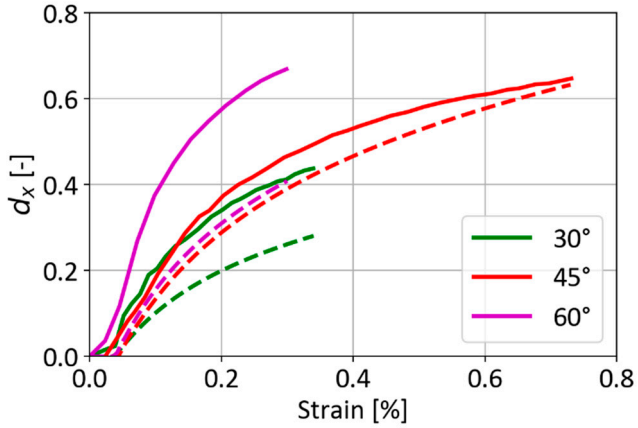

Figure 6. Comparison between damage curves obtained from experiments (solid line) and simulation (broken line) for C/C–SiC.

Now let us consider Figure 6, where damage, i.e., loss in the global stiffness of the material under tension, is plotted against strain applied on the material. It can be observed that the global damage (broken line) determined by the damage model in the case of ±45° is in good agreement with that of the damage evaluated from the experiment (solid line). However, in the case of ±30° and ±60°, damage is underestimated by the damage model. It is known from the previous discussion that the sample with ±30° and ±60° fiber orientations exhibits multiple damage modes. A combined effect of the damage modes is, however, not considered in the model. In other words, the presence of multiple damage modes results in a higher or accelerated loss of global stiffness when compared to the presence of a single damage mode in a laminate. For example, in the case of ±60°, damage in both the 2-direction and the 12-direction leads to an excess loss of stiffness and results in a non-linear curve which is not considered in the current damage model. There might be cracks in the matrix (presence of d_2) but the load is still carried by the shear stiffness provided by the presence of fibers in the matrix. Similarly, in the case of ±30°, an excess loss of stiffness takes place due to the presence of both d_1 and d_{12} in the laminate. This explains the discrepancy between the stress–strain curve obtained from the tensile experiment and the damage model. This is a shortcoming of the proposed damage model, and is a topic for future work where an interaction parameter will be introduced to ensure accelerated damage evolution in the case of the presence of multiple damage modes, as shown in Figure 7. The damage

surface in that case evolves faster under the presence of multiple stress components, when compared to the presence of a single dominating stress component. For example, in Figure 7, the damage evolution is enhanced when both Y_2 and Y_{12} are present in a particular load state when compared to a load state where only either Y_2 or Y_{12} is present.

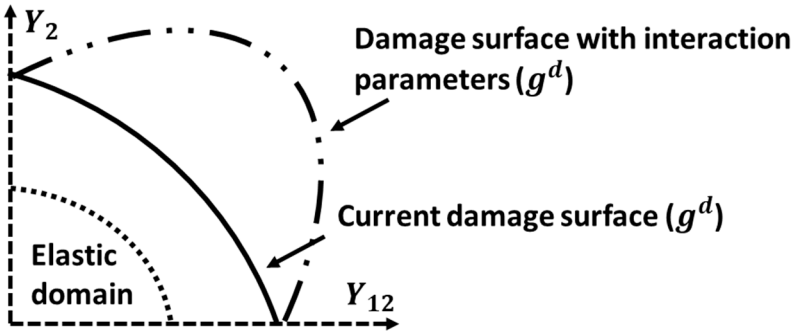

Figure 7. Damage surface with consideration of the interaction of damage parameters in the presence of multiple damage models in the thermodynamics space.

3.3.2. Iosipescu Shear Test

In-plane Iosipescu shear tests were performed in the work of Breede [27] and Shi [30] for materials C/C–SiC and WHIPOX™, respectively. However, the stress–strain curves obtained were valid only in the elastic region. The test turned out to be invalid for the determination of the shear strength of the material, as the sample did not fail in the expected notched area. For this reason, it is important to note that the stress and strain values where the curves end should not be considered as the strength of the laminate under pure shear loading. Nevertheless, a comparison between the stress–strain curves is shown in Figures 8 and 9 in order to demonstrate the non-linearity captured by the damage model.

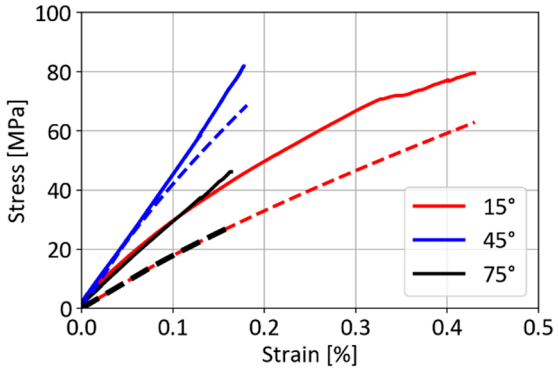

Figure 8. Comparison between the stress–strain curves obtained from the simulation (broken line) and Iosipescu shear tests (solid line) with different fiber orientations for C/C–SiC.

As observed in Figure 8, the shear stiffness of laminates with ±15° and ±75° within the initial elastic region is comparable in the case of C/C–SiC. This is in accordance with the classical laminate theory, and for this particular reason, the curves from the damage model overlap each other. Similarly, in the case of WHIPOX™ laminates (as seen in Figure 9), the curves overlap each other in the elastic region in these fiber orientations: ±22.5° and 67.5°; ±30° and ±60°.

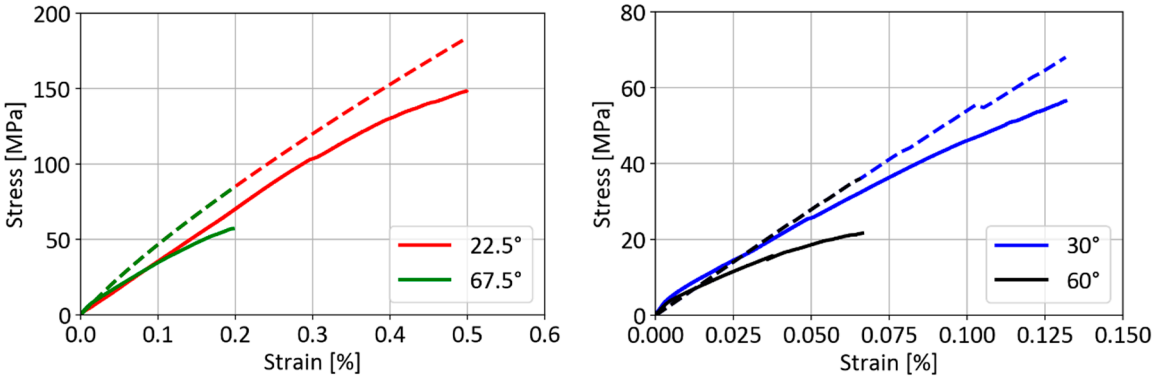

Figure 9. Comparison between the stress–strain curves obtained from simulation (broken line) and Iosipescu shear tests (solid line) with different fiber orientations for WHIPOX™. (**a**) ±22.5° and 67.5°; (**b**) ±30° and ±60°.

If pure shear stress is resolved into local stress components (σ_1, σ_2 and σ_{12}), it is observed that the matrix is under compressive stress (as seen in Figure 10). The damage model in the current work does not consider any loss of stiffness under compression, i.e., $d = 0$ and the Young's modulus remains constant throughout the test. Another assumption which is considered in the model is that the Young's modulus is the same under compression and tension, which might not be the case with CMCs, as shown in the earlier publication with WHIPOX™ [38].

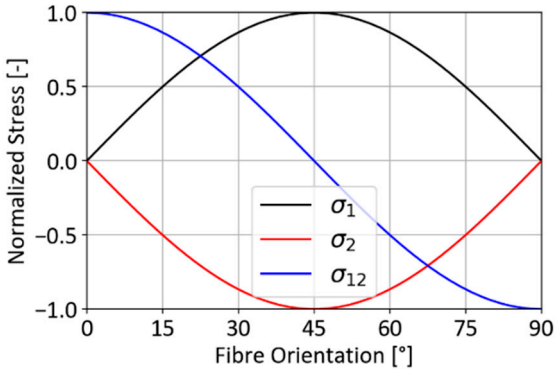

Figure 10. Normalized variation of local stress components after application of pure shear load on a laminate with given fiber orientation.

As discussed in the previous section, the Iosipescu shear test could not deliver the strength values for the laminates. However, the shear modulus could be accurately determined by the test, but the results were invalid for both the materials as soon as the material left the linear elastic region, i.e., as soon as crack evolution started in the laminate. This phenomenon raises the question of whether the Iosipescu test is an appropriate method to determine the shear strength of the material. The authors believe that due to the presence of notches in the sample, the strength of the material becomes a function of the shape and direction of the notch and the fiber orientation of the sample.

As shown in Figure 11, in case of ±15°, the crack might initiate from a region where the fibers are damaged while preparing the sample [39]. As the crack grows further, it gets deflected at the fiber boundary and moves along the fibers which are almost perpendicular to the direction of crack growth. In this manner, crack growth is hindered by the fibers and the crack follows a zig-zag path until it reaches the notch on the other side of the sample. This deflection of the crack leads to a higher amount of force required to fracture the sample, and consequently, the test gives a higher shear strength of the laminate. The C/C–SiC sample with ±15° fractured at a shear stress of 78 MPa. A similar phenomenon

was observed in the case of the WHIPOX™ sample with a fiber orientation of ±22.5°, where the crack is deflected on the fibers, which act as a hindrance to its movement (see Figure 12). On the other hand, in the case of ±75°, the notches are aligned in the fiber direction. When a crack initiates, as in the former case, it grows along the boundary of the fibers. The only difference is that the growth is not hindered by the fibers as they are aligned in the direction of the notch. Ultimately, the force required to fracture the sample is relatively low. The shear stress at the fracture of the sample with ±75° was evaluated to be 46 MPa. Theoretically, the fiber orientations ±15° and ±75° should exhibit the same stiffness and strength under pure shear loading. Due to the different crack growth behavior in the material in the Iosipesu test and the interdependence of the notch and fiber direction, it can be concluded that the Iosipescu shear test is not appropriate for the determination of the shear strength of CMCs.

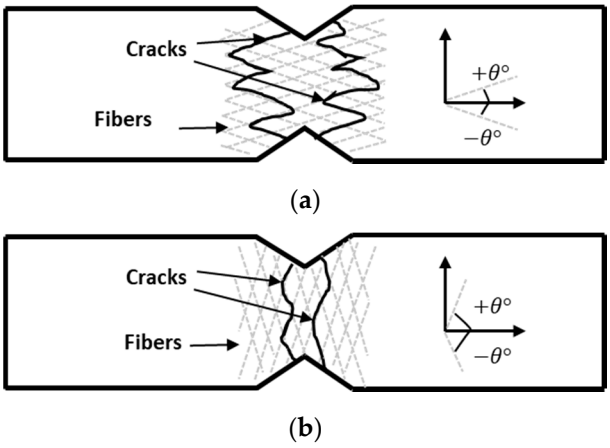

Figure 11. Crack growth in an Iosipescu test sample with fiber orientation (**a**) ±15° and (**b**) ±75°.

Figure 12. Crack growth in an Iosipescu test sample with fiber orientation of ±22.5° in the case of WHIPOX™ [30].

3.4. Tsai-Wu Failure Criterion

Similar to the determination of the representative elastic properties of a virtual UD layer in Section 3.2, the strength values are also fitted for a virtual UD layer. The maximum value for each component of the Tsai-Wu failure criterion in respective spaces (damage, strain or stress) is evaluated in such a way that the error percentage between the experimental values and the predicted values is minimum for all the fiber orientations. The results after the implementation of the Tsai-Wu failure criterion in different spaces are discussed in this section.

3.4.1. Damage-Space

Analogous to the stress-based Tsai-Wu failure criterion, the maximum values of damage are used to define a failure envelope. The maximum values used for the implementation of the failure criterion are summarized in Table 5.

Table 5. Damage limits for stress-based Tsai-Wu failure criterion.

Property	Unit	C/C–SiC	WHIPOX™
d_{1max}	-	0.30	0.025
d_{2max}	-	0.17	0.45
d_{12max}	-	0.70	0.43

A two-dimensional representation of the failure envelope in 3D space is shown in Figure 13. It has to be mentioned at this point that there are no negative values of damage. The region with negative values in Figure 13 is shown only in order to visualize the points that lie on the zero axis. According to the definition of damage, it can only be positive in a material. Starting with ±15° fiber orientation, 'purple triangle' takes the maximum value of d_1, which suggests that the sample fails due to damage in the 1-direction, i.e., fiber-dominant direction. On the other hand, the sample with ±75° fiber orientation fails due to damage in the 2-direction, i.e., the matrix-dominant direction, as 'black triangle' lies on the boundary of d_2. As expected, the sample with a ±45° orientation fails due to loss in the shear stiffness of the material and the point 'green square' lies on the maximum values of the d_{12} axis. The sample with a fiber orientation of ±30° exhibits combined damage modes. It ('red circle') takes maximum values for d_1 and can be seen on the boundary of the envelope in the $d_{12} - d_1$ axis. As discussed in the previous section, the damage in the laminate with the ±60° fiber orientation is underestimated by the model, and for this particular reason, 'blue triangle' lies outside the envelope. Because of the presence of both the d_2 and d_{12} damage modes, the interaction parameter for the damage-failure criterion will also be redefined in future work, just like the damage surface in thermodynamic space.

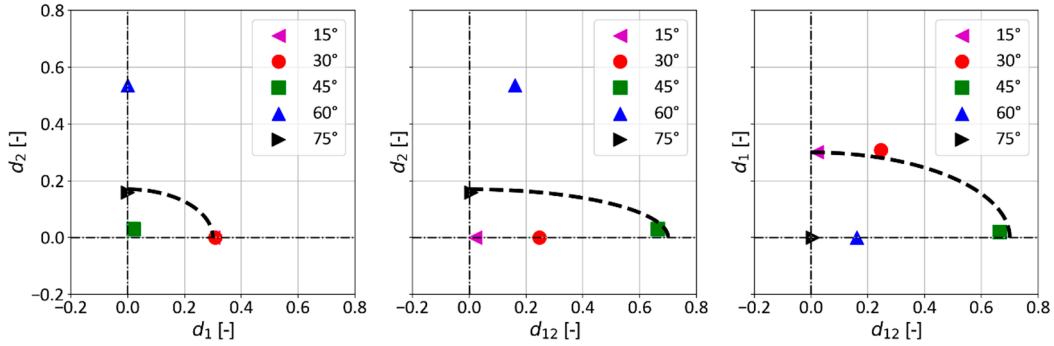

Figure 13. Two-dimensional representation of a 3D Tsai-Wu failure envelope for C/C–SiC with (**a**) d_1–d_2 axis, (**b**) d_{12}–d_2 axis and (**c**) d_{12}–d_1 axis with experimental results (markers) for different fiber orientations.

3.4.2. Stress-Space

The Tsai-Wu failure criterion is implemented in the stress-space for both the materials. The strength values used for the virtual UD layers are listen in Table 6. Due to lack of data under compression for C/C–SiC, the strength values under compression are taken to be the same as those of tension. The strength values for WHIPOX™ are taken from a previous work [11].

Table 6. Stress limits for stress-based Tsai-Wu failure criterion where superscripts 'T' and 'C' denote tension and compression, respectively.

Property	Unit	C/C–SiC	WHIPOX™ [11]
σ^T_{1max}	MPa	190	279
σ^T_{2max}	MPa	35	22.5
σ^C_{1max}	MPa	190	243
σ^C_{2max}	MPa	35	45
σ_{12max}	MPa	70	65

Figure 14 shows a comparison between the values obtained from the test and the predicted failure stress values. The damage-based failure criterion performed better than the stress-based criterion for all the fiber orientations for C/C–SiC, except in the case of ±60°. The value of d_{2max} (0.17) is reached at a very low value of stress in the case of ±60°. The damage limits are set in such a way that the error between the experimental results and the predicted values is minimum. Since d_{2max} influences the strength of ±45° and ±75° as well, a compromise had to be made in the case of the ±60° laminate.

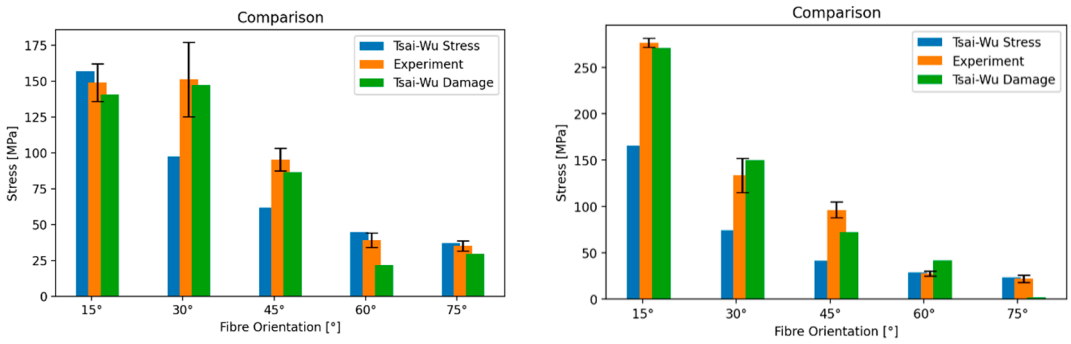

(**a**) (**b**)

Figure 14. Comparison of the failure stress values between the tensile test and the predicted values from the damage-based and stress-based Tsai-Wu failure criterion for (**a**) C/C–SiC and (**b**) WHIPOX™.

In the case of WHIPOX™, a good agreement can be found between the experimental results and the predicted values, with a low discrepancy in the case of ±45° and ±60° and a high discrepancy in the ±75° fiber orientation. As mentioned earlier, the value of d_{2max} is set in such a manner that the error between the experimental results and the failure criterion is minimum. Now, when the ±75° fiber orientation is observed, the value of d_{2max} is high when compared to the experimental results where the stress–strain curve is almost linear. The damage limit in the experiment is reached at a very low stress value in the damage model, and the predicted strength is also consequently low. On the other hand, in the ±60° laminate, the predicted damage is lower when compared to the experimental results and the damage limit is reached at a higher stress value. A compromise had to be made while determining the value of d_{2max}. In a similar way, the value of d_{2max} influences the strength of the ±45° laminate as well because of the presence of the σ_2 component.

3.4.3. Strain-Space

The Tsai-Wu failure criterion is implemented in the strain-space for both the materials. The strain limit values used for the virtual UD layers are listen in Table 7. The strain limit under compression is assumed to be same as under tension.

Table 7. Strain limits for strain-based Tsai-Wu failure criterion.

Property	Unit	C/C–SiC	WHIPOX™
ε_{1max}	%	0.20	0.15
ε_{2max}	%	0.10	0.023
ε_{12max}	%	0.70	0.60

Figure 15 shows a comparison between the values obtained from the test and the predicted failure strain values. The damage-based failure criterion performs even better in predicting failure strain than the strain-based Tsai Wu failure criterion. In the case of C/C–SiC, apart from ±60°, there is good agreement with the experimental results. As discussed in Section 3.3.1, the laminate with the ±60° fiber orientation exhibits extremely high non-linear behavior before fracture, and has a very high failure strain. With the inclusion of an interaction parameter in the failure criterion, the model should be able to predict failure strain with higher accuracy.

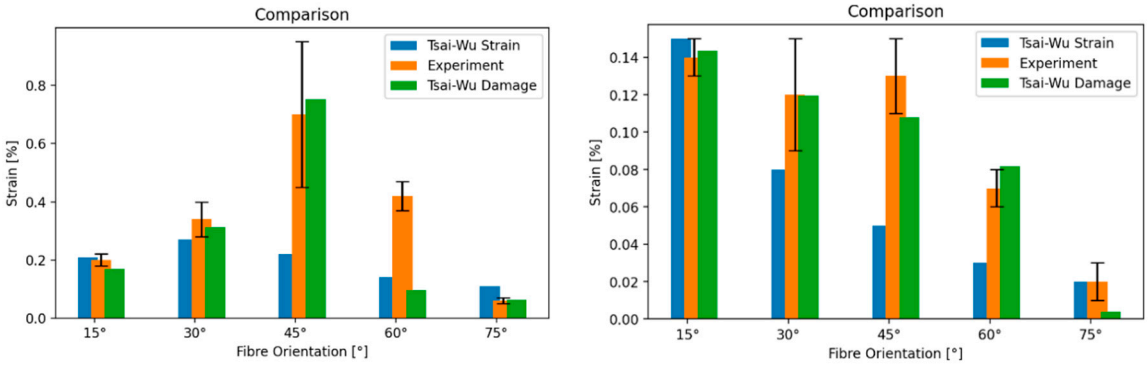

(**a**) (**b**)

Figure 15. Comparison of the failure strain values between the tensile test and the predicted values from the damage-based and strain-based Tsai-Wu failure criterion for (**a**) C/C–SiC and (**b**) WHIPOX™.

As far as WHIPOX™ is concerned, failure strain is predicted with a higher accuracy in comparison to Tsai-Wu in the strain-space as well. The discrepancy in the laminates with the ±45°, ±60° and ±75° fiber orientations is because of the same reason as discussed in the stress-space.

This comparison of the damage-based criterion with the Tsai-Wu failure criterion in stress- and strain-space demonstrates that it can predict the failure stress and strain with higher accuracy. It considers the losses in the Young's moduli and shear moduli, which are a result of changes in the microstructure of the material. In this manner, this criterion based on mechanical behavior at the macro-level can be correlated to the physical properties of the microstructure, such as increases in crack density with increasing load. In Shi et al. [11], two sets of UD strength limits were required to predict the strength of laminates with different fiber orientations with consideration of microstructural effects. The damage-based criterion, on the other hand, can predict the strength with one set of damage limits, as the microstructural information (loss of stiffness, i.e., increase in cracks) is already considered in the evaluation of damage. In this manner, the damage limits can be used as design limits by engineers while designing a component with complex a fiber-layup via filament winding, such as a nozzle [27].

4. Conclusions

In this work, an anisotropic damage model based on continuum mechanics is integrated with a damage-based failure criterion in order to predict the inelastic behavior of two ceramic matrix composites manufactured via filament winding technology. Damage in the material is defined as continuous stiffness reduction in the laminate with increasing load. As there were no test results available for unidirectional plies, the elastic properties of a virtual unidirectional ply were evaluated

from the tensile tests carried out on laminates with different fiber orientations. The parameters required for damage models were derived from the stress–strain curves obtained from tensile tests. The damage model was implemented in a commercial finite element software, ANSYS Workbench. It was observed that laminates with a fiber orientation where the fiber carries most of the load, e.g., ±15°, exhibit a relatively linear stress–strain curve compared to the matrix-dominant direction, e.g., ±60°. In this way, the inelastic behavior of laminates with varying fiber orientations can be predicted with a single parameter set for damage description.

In order to predict the failure stress and strain of laminates, a damage-based failure criterion inspired by the Tsai-Wu failure criterion was proposed. The failure criterion considers the coupling of damage variables in different directions, which makes it appropriate to be used for anisotropic CMCs. The predictions made by the damage-based criterion were closer to the experimental results in comparison to the stress- or strain-based Tsai-Wu failure criterion. Moreover, a damage-based criterion can be directly related to the physical attributes of a material, such as crack density, and has potential to give an insight into the micromechanics of the material despite its macroscopic nature.

The application of the proposed model on Iosipescu shear tests showed discrepancy when compared with the experimental results. All three in-plane stress components (tension, compression and shear) are present in the sample based on its fiber orientation. This discrepancy is attributed to the assumption that the material behaves linearly elastically under compression, i.e., no damage occurs under compression. The further investigation of the fracture surfaces of materials after failure led to the conclusion that the Iosipescu shear test can determine the shear modulus of the material, but is not an appropriate test to evaluate the shear strength of the material because of the interdependence of notches and the fiber orientation of the laminate.

The proposed damage-based failure criterion considers loss of stiffness in principal material directions, which can be used as design limits for a CMC component under thermomechanical loading and can differentiate between damage mechanisms under tension and compression. Loss of stiffness can be measured via non-destructive testing (NDT) methods, such as acoustic emissions, and can be used as a quality assurance criterion in order to determine the life cycle of a CMC component after being in operation for a definite period of time.

Author Contributions: Conceptualization, methodology, software, validation, investigation, visualization, writing—original draft preparation: N.J.; writing—review, supervision, funding acquisition: D.K. All authors have read and agreed to the published version of the manuscript.

Funding: The research was partially funded by Federal Ministry of Economic Affairs and Energy under the framework of project 'HOT_TCF' with grant number LUFOV1-549-009.

Acknowledgments: Authors would like to thank Yuan Shi for providing test data, discussions regarding its interpretation and for allowing them to use an image from his dissertation. Authors would also like to thank Swaroop G. Nagaraja from Institute of Mechanics, Montanuniversität Leoben for discussions regarding the continuum damage model.

Conflicts of Interest: The authors declare no conflict of interest.

References

1. Krenkel, W.; Berndt, F. C/C–SiC composites for space applications and advanced friction systems. *Mater. Sci. Eng. A* **2005**, *412*, 177–181. [CrossRef]
2. Kochendörfer, R.; Lutzenburger, N. Applications of CMCs made via the liquid silicon infiltration (LSI) technique. In *High Temperature Ceramic Matrix Composites*; Wiley-VCH: Weinheim, Germany, 2006; pp. 275–287.
3. GerendÁs, M.; Cadoret, Y.; Wilhelmi, C.; Machry, T.; Knoche, R.; Behrendt, T.; Aumeier, T.; Denis, S.; Göring, J.; Koch, D.; et al. Improvement of oxide/oxide CMC and development of combustor and turbine components in the HiPOC program. *Proc. ASME Turbo. Expo. 2011 GT2011* **2011**, 477–490. [CrossRef]
4. Behrendt, T.; Hackemann, S.; Mechnich, P.; Shi, Y.; Hönig, S.; Hofmann, S.; Koch, D. Development and test of oxide/oxide ceramic matrix composites combustor liner demonstrators for aero-engines. *J. Eng. Gas Turbines Power* **2016**, *139*, 031507. [CrossRef]

5. Stahl, V.; Shi, Y.; Kraft, W.; Lanz, T.; Vetter, P.; Jemmali, R.; Kessel, F.; Koch, D. C/C-SiC component for metallic phase change materials. *Int. J. Appl. Ceram. Technol.* **2020**, *17*, 2040–2050. [CrossRef]
6. Göring, J.; Hackemann, S.; Kanka, B. WHIPOX®: Ein faserverstärkter oxidkeramischer werkstoff für hochtemperatur—Langzeitanwendungen. *Mater. Und Werkst.* **2007**, *38*, 766–772. [CrossRef]
7. Breede, F.; Jemmali, R.; Voggenreiter, H.; Koch, D. Design and testing of a C/C-Sic nozzle extension manufactured via filament winding technique and liquid silicon infiltration. *Des. Dev. Appl. Struct. Ceram. Compos. Nanomater.* **2014**, *244*, 3–14.
8. Lamon, J. Interfaces and interfacial mechanics: Influence on the mechanical behavior of ceramic matrix composites (CMC). *J. Phys.* **1993**, *3*, 1607–1616. [CrossRef]
9. Marshall, D.B.; Cox, B.N.; Evans, A.G. The mechanics of matrix cracking in brittle-matrix fiber composites. *Acta Met.* **1985**, *33*, 2013–2021. [CrossRef]
10. Lamon, J. A micromechanics-based approach to the mechanical behavior of brittle-matrix composites. *Compos. Sci. Technol.* **2001**, *61*, 2259–2272. [CrossRef]
11. Shi, Y.; Jain, N.; Koch, D. Investigation and modeling of tensile failure properties of wound ceramic matrix composites. *Compos. Part A Appl. Sci. Manuf.* **2018**, *114*, 316–326. [CrossRef]
12. Baranger, E. 5.8 Modeling mechanical behavior of ceramic matrix composites. In *Comprehensive Composite Materials II*; Elsevier: Oxford, UK, 2018; pp. 237–268.
13. Wulfinghoff, S.; Fassin, M.; Reese, S. A damage growth criterion for anisotropic damage models motivated from micromechanics. *Int. J. Solids Struct.* **2017**, *121*, 21–32. [CrossRef]
14. Ladeveze, P.; LeDantec, E. Damage modelling of the elementary ply for laminated composites. *Compos. Sci. Technol.* **1992**, *43*, 257–267. [CrossRef]
15. Marcin, L.; Maire, J.-F.; Carrère, N.; Martin, E. Development of a macroscopic damage model for woven ceramic matrix composites. *Int. J. Damage Mech.* **2011**, *20*, 939–957. [CrossRef]
16. Camus, G. Modelling of the mechanical behavior and damage processes of fibrous ceramic matrix composites: Application to a 2-D SiC/SiC. *Int. J. Solids Struct.* **2000**, *37*, 919–942. [CrossRef]
17. Talreja, R. A continuum mechanics characterization of damage in composite materials. *Proc. R. Soc. Lond. Ser. A Math. Phys. Sci.* **1985**, *399*, 195–216.
18. Kumar, R.S. Analysis of coupled ply damage and delamination failure processes in ceramic matrix composites. *Acta Mater.* **2013**, *61*, 3535–3548. [CrossRef]
19. Barbero, E.J.; De Vivo, L. A constitutive model for elastic damage in fiber-reinforced PMC laminae. *Int. J. Damage Mech.* **2001**, *10*, 73–93. [CrossRef]
20. Hinton, M.; Soden, P.; Kaddour, A.-S. *Failure Criteria in Fibre Reinforced Polymer Composites: The World-Wide Failure Exercise*; Elsevier: Oxford, UK, 2004.
21. Petersen, E.; Cuntze, R.G.; Hühne, C. Experimental determination of material parameters in cuntze's failure-mode-concept-based UD strength failure conditions. *Compos. Sci. Technol.* **2016**, *134*, 12–25. [CrossRef]
22. Van Paepegem, W. Development and Finite Element Implementation of a Damage Model for Fatigue of Fibre-Reinforced Polymers. Ph.D. Thesis, Ghent University, Ghent, Belgium, 2002.
23. Tushtev, K.; Horvath, J.; Koch, D.; Grathwohl, G. Deformation and failure modeling of fiber reinforced ceramics with porous matrix. *Adv. Eng. Mater.* **2004**, *6*, 664–669. [CrossRef]
24. Yang, C.P.; Jiao, G.Q.; Wang, B.; Huang, T.; Guo, H.-B. Damage-based failure theory and its application to 2D-C/SiC composites. *Compos. Part A Appl. Sci. Manuf.* **2015**, *77*, 181–187. [CrossRef]
25. Krenkel, W. Entwicklung Eines Kostengunstigen Verfahrens zur Herstellung von Bauteilen aus Keramischen Verbundwerkstoffen. Ph.D. Thesis, Universität Stuttgart, Stuttgart, Germany, 2000.
26. Krenkel, W.; Hausherr, M.; Reimer, T.; Frieß, M. Design, manufacture and quality assurance of C/C-SiC composites for space transportation systems. In Proceedings of the 28th International Conference on Advanced Ceramics and Composites: B, Ceramic Engineering and Science Proceedings, Cocoa Beach, FL, USA, 1 January 2004; pp. 49–58.
27. Breede, F. Entwicklung Neuartiger Faserkeramischer C/C-SiC Verbundwerkstoffe auf Basis der Wickeltechnik für Raketendüsen. Ph.D. Thesis, German Aerospace Centre, Fakultät für Luft- und Raumfahrttechnik und Geodäsie, Universität Stuttgart, Stuttgart, Germany, 2017.
28. Schmücker, M.; Schneider, H. WHIPOX all oxide ceramic matrix composites. In *Handbook of Ceramic Composites*; Springer: Boston, MA, USA, 2005; pp. 423–435.

29. Schmücker, M.; Mechnich, P. All-Oxide ceramic matrix composites with porous matrices. In *Ceramic Matrix Composites*; Wiley-VCH: Weinheim, Germany, 2008; pp. 205–229.
30. Shi, Y. Characterization and Modeling of the Mechanical Properties of Wound Oxide Ceramic Composites. Ph.D. Thesis, Fakultät für Maschinenbau, Karlsruhe Institut für Technologie (KIT), Karlsruhe, Germany, 2017.
31. Barbero, E.J. *Finite Element Analysis of Composite Materials Using ANSYS®*; CRC Press: Boca Raton, FL, USA, 2013.
32. Koch, D.; Tushtev, K.; Grathwohl, G. Ceramic fiber composites: Experimental analysis and modeling of mechanical properties. *Compos. Sci. Technol.* **2008**, *68*, 1165–1172. [CrossRef]
33. Sikkil, K.K. Finite Element Damage Modeling of Plain WEAVE fabrics. Master of Science (M.Sc.)'s Thesis, Department of Mechanical and Aerospace Engineering, West Virginia University, College of Engineering and Mineral Resources, Morgantown, WV, USA, 2003.
34. Tsai, S.W.; Wu, E.M. A general theory of strength for anisotropic materials. *J. Compos. Mater.* **1972**, *5*, 58–80. [CrossRef]
35. Liu, K.-S.; Tsai, S.W. A progressive quadratic failure criterion for a laminate. *Compos. Sci. Technol.* **1998**, *58*, 1023–1032. [CrossRef]
36. Jones, R.M. *Mechanics of Composite Materials*; Taylor & Francis: Philadelphia, PA, USA, 1998.
37. Narayanaswami, R.; Adelman, H.M. Evaluation of the tensor polynomial and Hoffman strength theories for composite materials. *J. Compos. Mater.* **1977**, *11*, 366–377. [CrossRef]
38. Shi, Y.; Jain, N.; Jemmali, R.; Hofmann, S.; Koch, D.; Hackemann, S. Prediction of elastic properties for a wound oxide ceramic matrix composite material. *Int. J. Appl. Ceram. Technol.* **2015**, *12*, E99–E110. [CrossRef]
39. Spigel, B.S. An Experimental and Analytical Investigation of the Iosipescu Shear Test for Composite Materials. Master of Science (MS)'s Thesis, Mechanical & Aerospace Engineering, Old Dominion University, Norfolk, VA, USA, 1994.